J Infrared Milli Terahz Waves (2013) 34:42–52
DOI 10.1007/s10762-012-9947-1

Continuously Tunable 250 GHz Gyrotron with a Double Disk Window for DNP-NMR Spectroscopy

Sudheer Jawla · Qing Zhe Ni · Alexander Barnes · William Guss · Eugenio Daviso · Judith Herzfeld · Robert Griffin · Richard Temkin

Received: 6 June 2012 / Accepted: 29 October 2012 /
Published online: 15 November 2012

Abstract In this paper, we describe the design and experimental results from the rebuild of a 250 GHz gyrotron used for Dynamic Nuclear Polarization enhanced Nuclear Magnetic Resonance spectroscopy on a 380 MHz spectrometer. Tuning bandwidth of approximately 2 GHz is easily achieved at a fixed magnetic field of 9.24 T and a beam current of 95 mA producing an average output power of >10 W over the entire tuning band. This tube incorporates a double disk output sapphire window in order to maximize the transmission at 250.58 GHz. DNP Signal enhancement of >125 is achieved on a ^{13}C-Urea sample using this gyrotron.

Keywords Gyrotron · Double disk window · Frequency tunable · Gaussian beam · Waveguide

1 Introduction

Solid State Nuclear Magnetic Resonance (SS-NMR) spectroscopy is a powerful tool for investigating atomic-resolution structures and functions of biological macromolecules. Its wide applicability is illustrated by recent structural studies of microcrystalline – proteins, amyloid peptides and proteins, membrane proteins and non-protein molecular assemblies [1–13]. However, low sensitivity and spectral resolution have been a roadblock limiting its applications. Recent progress and the use of high frequency gyrotrons allow the sensitivity enhancement of NMR using Dynamic Nuclear Polarization (DNP) [14–17]. In high-field DNP experiments, large electron spin polarization from stable paramagnetic centers is transferred to the nuclear

S. Jawla (✉) · W. Guss · R. Temkin
Plasma Science and Fusion Center, Massachusetts Institute of Technology, Cambridge, MA 02139, USA
e-mail: sudheerjawla@gmail.com

Q. Z. Ni · A. Barnes · E. Daviso · R. Griffin
Francis Bitter Magnet Lab and Department of Chemistry, Massachusetts Institute of Technology, Cambridge, MA 02139, USA

E. Daviso · J. Herzfeld
Department of Chemistry, Brandies University, Waltham, MA 02454, USA

spin reservoir by manipulating the unpaired electron spins and exciting the Electron Paramagnetic Resonance (EPR) transitions with the use of high intensity microwave radiation at cryogenic temperatures thereby improving the sensitivity of NMR spectra by more than 100 fold and thus reducing the acquisition time in multidimensional magic-angle spinning NMR experiments [18–21]. This drives the effort of developing high frequency gyrotrons in the THz region producing few tens of watts of microwave power. Further optimization of the DNP resonance condition requires a frequency tunable source. This optimization of the resonance condition for the positive and negative enhancement maxima, defined by the nuclear Zeeman splitting, of various samples can be achieved either by varying the irradiating microwave frequency (f) or by changing the NMR magnetic field (B_{NMR}). The splitting amounts to Δf= 0.4 GHz or ΔB_{NMR}=14 mT for ^{1}H at B_{NMR}=9.3 T. The separation of the enhancement maxima depends on the concentration of the radical compounds and the type of nuclear species. The frequency tunability of the gyrotron eases the optimization of the resonance condition by avoiding the need for sweeping the field of the NMR magnet which helps us to overcome several cumbersome steps e.g. changing the main coils/auxiliary sweep coil (disturbs the homogeneity of the field), inspecting the sweep width with the field strength and tuning of the RF circuits for different nuclei every time the NMR field is adjusted [22].

We have previously built gyrotrons at 140, 250, 330 and 460 GHz for DNP-NMR spectrometers at 211, 380, 500 and 700 MHz respectively [23–29]. The gyrotrons at 330 and 460 GHz [27, 28] are frequency tunable with >1 GHz of tuning bandwidth and capable of producing a maximum of ~20 W of power at a single frequency and ≥~ 5 W of average power over the entire tuning bandwidth. Other research groups are also actively developing gyrotrons and instrumentation for DNP-NMR at frequencies moving to higher magnetic field [30–35] targeting large and complex molecular systems. Recently, the highest field DNP-NMR system has been installed at MIT to perform MAS DNP at 700 MHz / 460 GHz [36]. Initial enhancement of −40 at 5.6 kHz of spinning frequency was observed for ^{13}C-Urea.

In this work, we present the design and experimental results of a rebuild of our 250 GHz gyrotron for the 380 MHz NMR spectrometer. The original 250 GHz gyrotron at MIT operated in the TE_{03} mode and produced up to 25 Watts [24]. Following many years of operation, a new tube was built in the TE_{52} mode and operated at 8.5 to 12.5 kV and currents of up to 190 mA. An output power level of about 10 Watts was achieved over a bandwidth of close to 3 GHz near 250 GHz [37]. However, it was discovered that the output window of the gyrotron was a single sapphire disk that by mistake was not the proper thickness for the design frequency and was also cut along the wrong crystal axis of the sapphire. Very large reflections from the window caused internal overheating and ultimately led to a second rebuild of the gyrotron with further improvements. In this paper, we report on an improvement to the gyrotron which uses a double disk window to overcome the problems of the single sapphire disk. We have successfully integrated the window into the previous design [37], resulting in a frequency tunable 250 GHz gyrotron with ~2 GHz of frequency bandwidth and producing ~30 W of peak microwave power and >10 W of average power over the entire band. The tunability around the central frequency of 250 GHz was achieved by exciting the higher order longitudinal modes ($TE_{5,\,2,\,q}$ q>1) interacting with the backward wave components of the field excited in the resonator cavity by varying the operating magnetic field and voltage.

2 Design and Fabrication

The need for wide tunability i.e. to generate a>1 MHz nutation frequency across the entire nitroxide EPR lineshape for cross effect DNP, as well as to excite solid effect transitions

utilizing different radicals without the need for sweeping the NMR magnetic field have been the major requirements for implementing the gyrotron [37]. This tube is a modification from its previous version aiming for improvements in terms of the output power.

The design of the previous gyrotron [37] includes the selection of the operating mode, the cavity profile design and the electron gun design. Figure 1 shows a schematic of the frequency tunable 250 GHz gyrotron and the complete 380 MHz NMR spectrometer installed in the same room. The gyrotron consists of a diode type magnetron injection gun (MIG) with an emitter radius of 5.38 mm. The electron gun was previously designed for the first version of the gyrotron using code EGUN. The beam parameters were again verified using the commercial code MICHELLE. The beam pitch factor α evolution with respect to voltage is shown in Fig. 2. The high voltage power supply produces up to 200 mA of beam current for cathode bias voltages up to 15 kV and generating a beam power of ~3 kW. The cathode uses a traditional M-type dispenser emitter.

During the design of the interaction cavity, a set of higher order TE modes were examined for strong coupling to the electron beam. The cavity dimensions were established using a cold cavity code [38]. The cavity geometry consisted of three sections; a downtaper at 3 degrees, a straight resonator section of radius 2.018 mm and length ~19λ, λ being the wavelength, followed by an uptaper section at 0.4 degrees. The cavity length was chosen as a compromise between the advantages of a shorter cavity, such as lower diffractive quality factor (Q_d), against the advantages of a longer cavity, such as enhanced interaction efficiency and lower starting current. The cavity was designed to operate in a single mode $TE_{5,2}$ at the fundamental harmonic because this mode avoids mode competition with nearby modes and because of its high coupling to an electron beam of radius r_e=1.02 mm. Mode competition with the nearby modes was avoided and high electron beam coupling efficiency was obtained by optimizing the beam radius and the cavity dimensions. The starting currents of the desired mode and its neighboring modes were computed using linear theory assuming a Gaussian axial field profile in the cavity. These calculations showed sufficient mode separation between the main mode $TE_{5,2,q}$ and the nearby modes [37]. The design parameters are listed in Table 1. The calculated frequency tunability of more than 2 GHz around the nominal frequency was established using

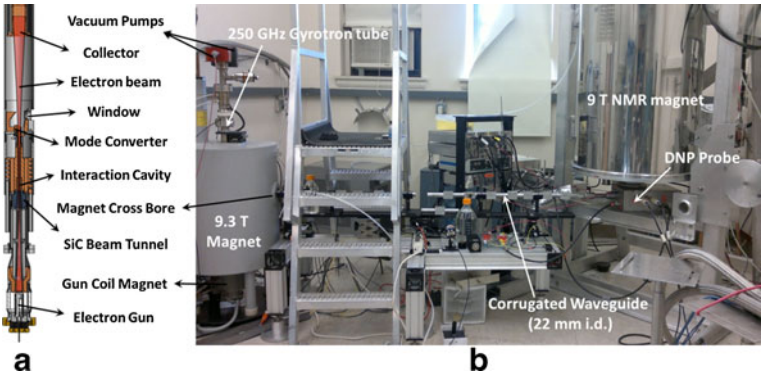

Fig. 1 **a**) Drawing view of the frequency-tunable 250 GHz gyrotron. **b**) Gyrotron in a 9.3 T superconducting magnet and NMR spectrometer and their related components as installed at the Francis Bitter Magnet Lab, MIT.

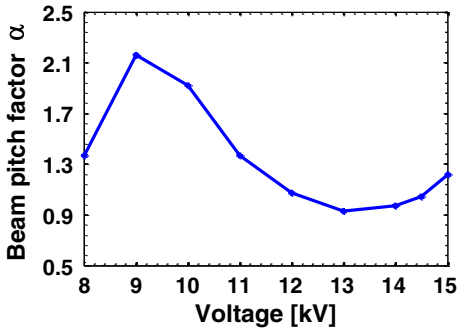

Fig. 2 Beam pitch factor α variation with respect to the operating voltage at a magnetic field of 9.3 T.

the self-consistent code MAGY [39]. The tunability is achieved by exciting the higher order longitudinal modes $TE_{5,2,q}$ (q=1–7). Modes with different axial number q provide a continuous tuning range since their eigenfrequencies are closer to each other. We have demonstrated such tunability in previous experiments using 330 GHz and 460 GHz gyrotrons [27, 28].

The design incorporates a Vlasov type internal quasi-optical mode converter designed to convert the cavity mode $TE_{5,2}$ to a Gaussian beam at the output window [40]. Figure 3 shows a schematic of the mode converter assembly showing the helically cut launcher with an off-axis parabolic mirror and two concave mirrors. Figure 3 also shows the double disk window assembly and the outer tube which is novel to this gyrotron. The window incorporates two sapphire disks. The first disk (thickness 2.073 mm) was brazed onto a Kovar / stainless steel composite and e-beam welded onto the outer tubing. The second disk (thickness 2.294 mm and cut along the c-axis of the sapphire) was placed adjacent to the first disk with a spacing of 1.72 mm. The spacing between the two disks was chosen to maximize the microwave transmission at 250.58 GHz with a bandwidth of ~2 GHz and to have over 85 % transmission. The correct spacing was calculated using reflectance and transmittance theory for a layered medium. The second disk was assembled in such a manner that the spacing could be changed with minimal effort to maximize the transmission at different frequencies near the far ends of the tuning curve (Fig. 5). The double disk window has been successfully employed in the past to improve the matching at the output window [41].

Table 1 Gyrotron design parameters.

Nominal Frequency	250 GHz
Operating Mode	$TE_{5,2,q}$
Frequency Tuning	>2 GHz
Voltage V_b	<15 kV
Current I_b	<0.2 A
Output Peak Power	>35 W
Pitch factor α	1.8
Beam radius r_e	1.02 mm
Cavity radius r_c	2.018 mm
Resonator cavity length	23 mm
Uptaper angle θ_d	0.4 degrees

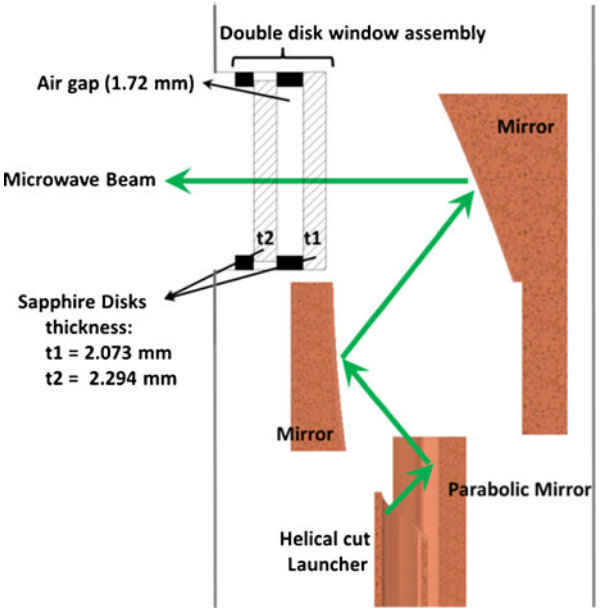

Fig. 3 Drawing picture of the double disk sapphire window assembly and Vlasov type mode converter assembly showing the helical cut launcher with off-axis parabolic mirror, two concave mirrors and the outer support tube.

3 Experimental Results

3.1 Double Disk Cold Test Results

We performed cold test measurements of the reflection S_{11} and transmission S_{21} on the single disk and double disk window using a Vector Network Analyzer (VNA, Agilent E8363B with millimeter wave extender V03VNA2-T/R). The reflection spectrum was measured from 230 GHz to 270 GHz. A linearly polarized input beam for testing was obtained from the combination of waveguide transitions and a corrugated horn (Thomas Keating Ltd., UK). The corrugated horn was then placed close to the window and aligned so as to produce a beam size at the window equal to the expected value from the internal mode converter. Figure 4 shows the theoretical and measured S_{11} spectrum for the double disk, after the final assembly of the gyrotron, ranging from 230 GHz to 270 GHz. Excellent agreement can be seen between the theoretically calculated and measured S_{11} for double disk from 245 GHz to 255 GHz. A small deviation in the agreement between theory and measurement on each side of the desired frequency can be ascribed to various factors e.g. small misalignment (not exactly parallel) in the window and horn aperture causing small fluctuations, beam waist lying at the horn aperture and not at the window, and reflections from the mode converter and inner tube components not properly coupling back to the horn. At the desired frequency of 250.58 GHz for the double disk window the theoretically simulated reflection matches very well with the measured S_{11} giving <3 % reflected power. The reflection over the desired bandwidth of ~2 GHz was <15 %. This indicates that in case of gyrotrons with larger tunability it is more advantageous to have a double disk window compared to a single disk because the user can optimize the spacing between the two disks for maximum transmission at the desired frequency.

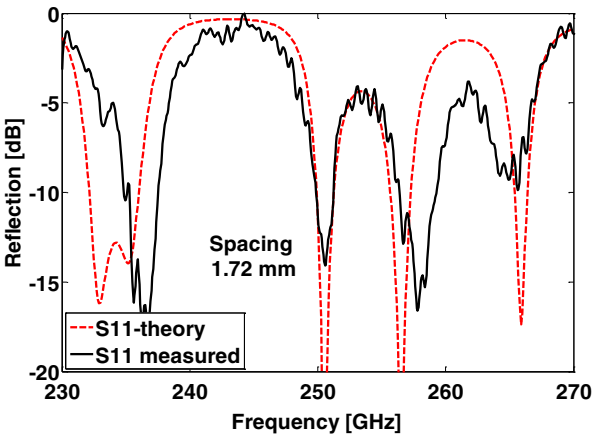

Fig. 4 Cold test measurements of the reflection S_{11} for double disk sapphire windows using a VNA. Double disk reflection measurement (*solid black curve*), and, theoretical reflection (*dashed red curve*) with 1.72 mm spacing between the two disks optimized for maximum transmission at 250.58 GHz.

3.2 Frequency Tunability

The gyrotron tube was continuously evacuated by two ion pumps (Fig. 1) to maintain the vacuum in the tube at levels of the order of 10^{-9} Torr during the operation. The electron beam collector, the gun coil magnet and resonator cavity were cooled with a chiller water circulator. The frequency of the radiation was varied continuously by tuning the voltage and magnetic field at the gyrotron cavity using programmable power supplies. Acceleration voltages were a modest 8–13 kV on the cathode. The MIG was operated with moderate electron beam currents in the range 50–150 mA. The pump controllers of the two ion pumps and the power supplies for the cathode, the gun-coil and the magnet were all mounted in a single 19" rack. The beam output power and frequency were stabilized within±1 % and <3 MHz respectively using a PID feedback control of the cathode heater, taking advantage of the LABVIEW software. The output microwave beam from the gyrotron was directly coupled to an overmoded corrugated circular waveguide transmission line consisting of 16 sections of 22 mm i.d. (made of Aluminum), each 15 cm long and a 4 port directional coupler [42]. The wave was subsequently transmitted over 2.4 m using this corrugated transmission line and fed into the DNP probe at the bottom of the NMR magnet (shown in Fig. 1) which has a mirror optics unit and a 0.58 m long 8 mm i.d. corrugated copper waveguide. Before the entry to the magic-angle sample spinning module, a miter bend was used to divert the microwave beam to the sample which is approximately 10 mm away from the sample rotor [43]. The microwave beam irradiates the sample transversely across the solenoidal NMR detection coil.

Figure 5 shows the measured frequency and output power of the radiation from the gyrotron as a function of the operating voltage at a constant magnetic field of 9.24 T. The figure also show the simulated output power (divided by 2) using the self-consistent code MAGY, and, voltage range where different axial modes are excited. The calculated output power is ~2.5 times higher than the measured power. This is not fully understood, however, in the previous version of the tube [23] thermal measurements indicated that cavity ohmic losses are higher than expected. It is more convenient to achieve the frequency tuning at a constant magnetic field by varying the

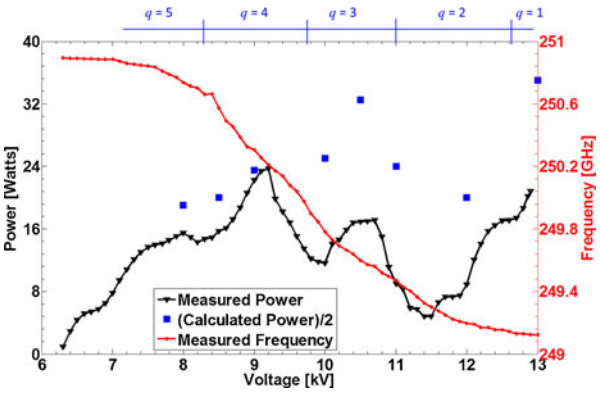

Fig. 5 Output power and frequency of the microwave radiation as a function of the operating voltage at a constant magnetic field of 9.24 T. The beam current was maintained at 95 mA. Blue squares represents the simulated power, divided by 2, using self-consistant code MAGY. Voltage range for the different longitudinal modes is also shown.

operating voltage, compared to varying the magnetic field at a constant voltage. The frequency of the radiation was measured with a heterodyne measurement system consisting of a detector diode/diplexer and a local oscillator (18 – 26 GHz range).

The output power was measured using a calibrated detector diode and a calorimeter connected to a power meter. We observed a frequency ranging from 249.1 GHz to 250.9 GHz, i.e. ~ 1.8 GHz tuning, by varying the operating voltage from 13.5 kV to 6.3 kV respectively. From 12 kV to 8 kV operating voltage the frequency variation was almost linear with ~1.5 GHz tuning. The average output power was >10 W over the 1.5 GHz tuning range with peak output power of 23 W at 9.2 kV and 250.21 GHz. The beam current was maintained at 95 mA during the entire operation using the PID controller. The cavity temperature was regulated at 18 °C using a chiller water circulator to avoid a frequency shift due to thermal expansion. Further tuning can be achieved by changing the magnetic field. A combination of magnetic field (9.01 T to 9.26 T) and voltage variation (8.5 kV to 13.5 kV) resulted in larger tuning bandwidths of ~3 GHz [37]. This bandwidth was larger than the high transmission window bandwidth (~ 2 GHz for >85 % transmission). Outside this range, reflections inside the gyrotron cause heating and unstable operation which results in lower efficiency and lower output power. The output power was also measured for different beam currents at fixed voltage and magnetic field which in turn fix the operating frequency. Figure 6 show the output power at three different voltage regions 8.51, 9.2 and 11.4 kV on the power curve shown in Fig. 5 which corresponds to 250.587, 250.21 and 249.362 GHz respectively. This is measured in order to have the output power reference with respect to the beam current for the NMR signal enhancement spectrum as a function of microwave power.

The alignment of the corrugated waveguide with respect to the gyrotron output window inside the cross bore of the magnet was critical for achieving higher transmission efficiency and therefore larger microwave power at the NMR sample. The output microwave beam profile at the window (inside the cross-bore) was measured using thermal paper for different exposure times showing a circular beam resulting in a high Gaussian beam content. The overmoded corrugated waveguide was then aligned at the window for maximum coupling by measuring the beam pattern using thermal paper and a pyroelectric camera (Spiricon III) after 1.2 m of corrugated waveguide. The alignment was done at the frequency 250.58 GHz. Figure 7 shows the beam profile measured using the pyroelectric camera at 4 cm in air from the waveguide aperture for two different operating frequencies on the ends of the tuning

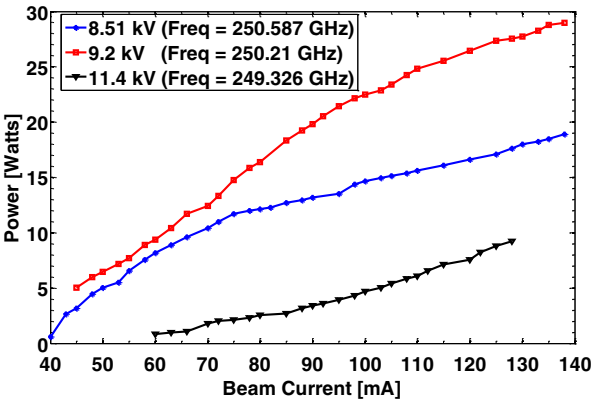

Fig. 6 Output microwave power as a function of the beam current at fixed operating voltages of 8.51 kV (250.587 GHz), 9.2 kV (250.21 GHz) and 11.4 kV (249.326 GHz) at a constant magnetic field of 9.24 T.

band, 249.18 and 250.58 GHz respectively. A clear difference is observed in the beam profile at the two frequencies. Different beam patterns at different frequencies affected the coupling to the corrugated waveguide and provided different transmission loss in the whole quasi-optical transmission line from gyrotron output window to the NMR sample.

Hot test transmission measurements were performed on the complete DNP probe assembly at 250.58 GHz in order to estimate the amount of power reaching the sample. The entire quasi-optical transmission line from the gyrotron output window to the NMR sample inside the NMR magnet consists of 2.4 m of 22 mm i.d. corrugated waveguide, a 4 port directional coupler, mirror optics unit in the probe, 0.58 m of 8 mm i.d. corrugated waveguide, miter-bend and a teflon lens [43]. The transmission efficiency was observed to be~40 %. Most of the losses occurred in the mirror transfer assebmly and the smaller diameter waveguide inside the NMR probe assembly. The loss in the 22 mm diameter corrugated waveguide is less than 0.03 dB/m [42, 44]. An elliptical beam profile at the sample location was observed by using a teflon lens at the end section of the miter-bend after the 8 mm diameter corrugated waveguide. The lens was used to transform the beam to an elliptical profile for maximum coupling to the sample through the optimized wire thickness of the RF coils surrounding the sample inside the stator housing [43].

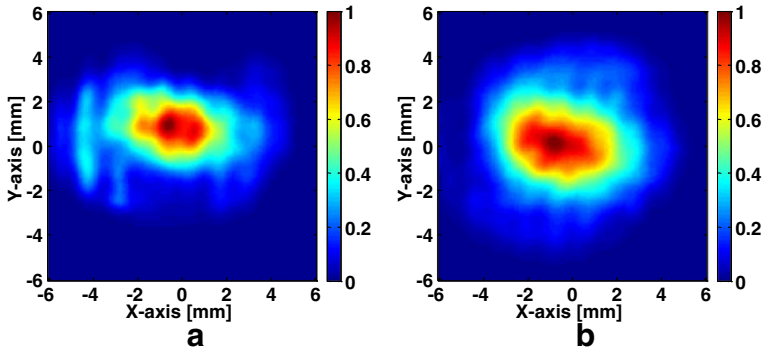

Fig. 7 Beam profile measured using a pyrocam at 4 cm in air radiated from the waveguide aperture at 1.2 m from the gyrotron output window at two different frequencies, **a**) 249.18, and, **b**) 250.58 GHz respectively.

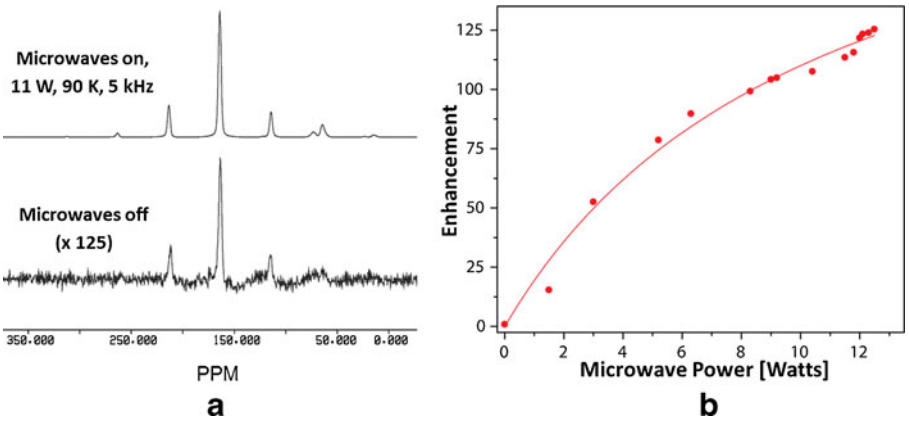

Fig. 8 **a**) Enhancement spectra for ^{13}C-Urea dissolved in a 60/30/10 glycerol/D_2O/H_2O glass forming matrix containing 10 mM TOTAPOL and 5 kHz spinning frequency. **b**) Microwave power vs enhancement for the ^{13}C-Urea sample.

4 DNP-NMR Results

DNP experiments were performed with a 380 MHz/250 GHz spectrometer. Figure 8a shows an enhancement of >125 on 1 M ^{13}C-Urea dissolved in a 60/30/10 glycerol d8/D_2O/H_2O glass forming matrix containing 10 mM TOTAPOL biradical polarizing agent [13, 18]. The sample solution was center packed in a 4 mm sapphire rotor. The sample temperature was detected by placing the temperature sensor right above the coil and rotor for accurate readings. By using the heat exchanger to cool the input nitrogen gas in bearing and drive, and the temperature control unit (Lakeshore) to provide heat using calibrated PID values when needed, the temperature was maintained at 90 K. The power dependence plot shown in Fig. 8b was also recorded at 5 kHz spinning frequency and reaches enhancement of 125 with ~12 W output power. The positive slope of the enhancement on microwave power indicates that further increase in power will likely lead to a higher enhancement factor [43]. In addition, temperatures of 80 K can be reached for future experiments, which would also greatly affect the enhancement value.

5 Conclusions

A 250 GHz gyrotron with ~2 GHz bandwidth and >10 W average output power with ~30 W peak power at 250.21 GHz has been successfully modified and integrated with a 380 MHz DNP-NMR spectrometer. The frequency tunability was conveniently achieved by varying the operating voltage from 7 kV to 13.5 kV at fixed magnetic field of 9.24 T. In order to further explore the frequency tunability range, the magnetic field and operating voltage can be varied in combination. A second sapphire disk is placed onto the first disk with 1.72 mm spacing between the two disks in order to maximize the transmission at 250.58 GHz which is verified by cold test measurements and showed excellent agreement with theory. We can optimize the spacing between the two disks to maximize the transmission at the desired frequency. DNP enhancements of >125 for ^{13}C-Urea were achieved at moderate microwave

power levels of ~12 W. Larger enhancements are likely at higher microwave power levels because the observed enhancements had not saturated and was limited by the gyrotron output power.

Acknowledgements This research was supported by the National Institutes of Health through grants EB002804, EB003151, EB002026, EB001960, EB001035, EB001965, and EB004866. We also thank Ivan Mastovsky for helping during the fabrication and assembling of the components.

References

1. C. Jaroniec, C. MacPhee, V. Bajaj, M. McMahon, C. Dobson, R. Griffin, *Proc. Natl. Acad. Sci.* 101 (2004) 711–716.
2. A. Petkova, Y. Ishii, J. Balbach, O. Antzutkin, R. Leapman, F. Delaglio, R. Tycko, *Proc. Natl. Acad. Sci.* 99 (2002) 16742.
3. R. Tycko, *Curr. Opin. Struct. Biol.* 14 (2004) 96–103.
4. M. Bayro, T. Maly, N. Birkett, C. MacPhee, C. Dobson, R. Griffin, *Biochemistry* 49 (2010) 7474–7488.
5. F. Creuzet, A. McDermott, R. Gebhard, K. van der Hoef, M. Spijker-Assink, J. Herzfeld, J. Lugtenburg, M. Levitt, R. Griffin, *Science* 251 (1991) 783–786.
6. Y. Li, D. Berthold, R. Gennis, C. Rienstra, *Protein Sci.* 17 (2008) 199–204.
7. A. Nevzorov, S. Park, S. Opella, *J. Biomol. NMR* 37 (2007) 113–116.
8. S. Cady, C. Goodman, C. Tatko, W. DeGrado, M. Hong, *J. Am. Chem. Soc.* 129 (2007) 5719–5729.
9. S. Cady, M. Hong, *Proc. Natl. Acad. Sci.* 105 (2008) 1483–1488.
10. J. Moffat, V. Vijayvergiya, P. Gao, T. Cross, D. Woodbury, D. Busath, *J. Biophys.* 94 (2008) 434–445.
11. Z. Song, F. Kovacs, J. Wang, J. Denny, S. Shekar, J. Quine, T. Cross, *J. Biophys.* 79 (2000) 767–775.
12. S. Kim, S. Matsuoka, G. Patti, J. Schaefer, *Biochemistry* 47 (2008) 3822–3831.
13. A.B. Barnes, G. De Paëpe, P. van der Wel, K. Hu, C. Joo, V. Bajaj, M. Mak-Jurkauskas, J. Sirigiri, J. Herzfeld, and R. Temkin, *Applied magnetic resonance* 34 (2008) 237–263.
14. L.R. Becerra, G.J. Gerfen, R.J. Temkin, D.J. Singel, and R.G. Griffin, *Phys. Rev. Lett.* 71 (1993) 3561–3564.
15. G. Gerfen, L. Becerra, D. Hall, R. Griffin, R. Temkin, D. Singel, *J. Chem. Phys.* 102 (1995) 9494–9497.
16. V.S. Bajaj, C.T. Farrar, M.K. Hornstein, I. Mastovsky, J. Vieregg, J. Bryant, B. Elena, K.E. Kreischer, R.J. Temkin, and R.G. Griffin, *J. Magn. Reson.*, 160 (2003) 85–90.
17. M. Rosay, V. Weis, K.E. Kreischer, R.J. Temkin, and R.G. Griffin, *J. Am. Chem. Soc. Society* 124 (2002) 3214–3215.
18. V. Bajaj, M. Mak-Jurkauskas, M. Belenky, J. Herzfeld, and R. Griffin, *Proc. Natl. Acad. Sci.* 106 (2009) 9244.
19. A. B. Barnes, B. Corzilius, M. Mak-Jurkauskas, L. Andreas, V. Bajaj, Y. Matsuki, M. Belenky, J. Lugtenburg, J. Sirigiri, R. Temkin, J. Herzfeld, and R.G. Griffin, *Phys. Chem. Chem. Phys.* 12 (2010) 5861–5861
20. M. Rosay, A.C. Zeri, N.S. Astrof, S.J. Opella, J. Herzfeld, and R.G. Griffin, *J. Am. Chem. Soc.* 123 (2001) 1010–1011.
21. M.L. Mak-Jurkauskas, V.S. Bajaj, M.K. Hornstein, M. Belenky, R.J. Temkin, R.G. Griffin, and J. Herzfeld, *Proceedings of the National Academy of Sciences of the United States of America* 105 (2008) 883–888.
22. Y. Matsuki, K. Ueda, T. Idehara, R. Ikeda, K. Kosuga, I. Ogawa, S. Nakamura, M. Toda, T. Anai, and T. Fujiwara, *J. Infrared and Millimeter Waves.* 33 (2012) 745–755.
23. K.E. Kreischer, C. Farrar, R.G. Griffin, R.J. Temkin, and J. Vieregg, *Proceedings of the 24th International Conference on Infrared and Millimeter Waves*, L. Lombardo, (Ed.), UC Davis, Monterey, CA, 1999, pp. TU-A3.
24. V.S. Bajaj, M.K. Hornstein, K.E. Kreischer, J.R. Sirigiri, P.P. Woskov, M. Mak, J. Herzfeld, R.J. Temkin, and R.G. Griffin, *J. Magn. Reson.*, 190 (2007) 86–114.
25. M.K. Hornstein, V.S. Bajaj, R.G. Griffin, K.E. Kreischer, I. Mastovsky, M.A. Shapiro, J.R. Sirigiri, and R.J. Temkin, *IEEE Trans. on Electron Devices* 52 (2005) 798–807.
26. S.T. Han, R.G. Griffin, K.N. Hu, C.G. Joo, C.D. Joye, J.R. Sirigiri, R.J. Temkin, A.C. Torrezan, and P.P. Woskov, *IEEE Trans. on Plasma Science* 35 (2007) 559–564.
27. A.C. Torrezan, S.T. Han, I. Mastovsky, M.A. Shapiro, J.R. Sirigiri, R.J. Temkin, A.B. Barnes, and R.G. Griffin, *IEEE Trans. on Plasma Science*, 38 (2010) 1150–1159.

28. A. C. Torrezan, M. A. Shapiro, J. R. Sirigiri, R. J. Temkin, and R. G. Griffin, *IEEE Trans. Electron Devices*, vol. 58, no. 8, pp. 2777–2783, Aug. 2011.
29. E.A. Nanni, A.B. Barnes, R.G. Griffin, and R.J. Temkin, *IEEE Trans. on Terahertz Science and Technology*, 1 (2011) 145–163.
30. Toshitaka Idehara, Kosuke Kosuga, La Agusu, Ryosuke Ikeda, Isamu Ogawa, et al., *Journal of Infrared, Millimeter and Terahertz Waves*, Volume 31, Number 7, Pages 775–790, 2010.
31. V. Denysenkov, M. J. Prandolini, M. Gafurov, D. Sezer, B. Endeward, and T. F. Prisner, *Physical Chem. Chemical Phys.*, vol. 12, no. 22, pp. 5786–5790, 2010.
32. U. Akbey, W. T. Franks, A. Linden, S. Lange, R. G. Griffin, B.-J. van Rossum, and H. Oschkinat, *Ang. Chem. Int.* vol. 49, no. 42, pp. 7803–7806, 2010.
33. Y. Matsuki, H. Takahashi, K. Ueda, T. Idehara, I. Ogawa, M. Toda, H. Akutsu, and T. Fujiwara, *Physical Chem. Chemical Phys.*, vol. 12, no. 22, pp. 5799–5803, 2010.
34. M. Rosay, L. Tometich, S. Pawsey, R. Bader, R. Schauwecker, M. Blank, P. M. Borchard, S. R. Cauffman, K. L. Felch, R. T. Weber, R. J. Temkin, R. G. Griffin, and W. E. Maas, *Physical Chem. Chemical Phys.*, vol. 12, no. 22, pp. 5850–5860, 2010.
35. V. Vitzthum, M. A. Caporini, and G. Bodenhausen, *J. Magn. Reson.*, vol. 205, no. 1, pp. 177–179, 2010.
36. A. B. Barnes, E. Markhasin, E. Daviso, V. K. Michaelis, E. Mena, R. DeRocher, A. Thakkar, E. A. Nanni, S. Jawla, P Woskov, J. Herzfeld, R. J. Temkin, R. G. Griffin, *J. Magn. Reson.* (2012), vol. 224, pp. 1–7.
37. A. B. Barnes, E. A. Nanni, J. Herzfeld, R. G. Griffin, R. J. Temkin, *J. Magn. Reson.* (2012), vol. 221, pp. 147–153.
38. A. W. Fliflet and M. E. Read, *Int. J. Electron.*, vol. 51, no. 4, pp. 475–484, 1981.
39. M. Botton, T.M. Antonsen Jr, B. Levush, K.T. Nguyen, and A.N. Vlasov, *IEEE Trans. on Plasma Science*, 26 (1998) 882–892.
40. S. N. Vlasov, L. I. Zagryadskaya, and M. I. Petelin, *Radio Eng. Electron. Phys.*, vol. 12, no. 10, pp. 14–17, 1975.
41. K. Felch, M. Blank, P. Borchard, T. S. Chu ; J. Feinstein, H. R. Jory, J. A. Lorbeck, C. M. Loring, Y. M. Mizuhara, J. M. Neilson, R. Schumacher, R. J. Temkin, *IEEE Trans. on Plasma Science*, Vol. 24 , pp. 558 – 569 (1996).
42. P.W. Woskov, V.S. Bajaj, M.K. Hornstein, R.J. Temkin, and R.G. Griffin, *IEEE Trans. on Microwave Theory and Techniques*, 53 (2005) 1863–69.
43. E.A. Nanni, A.B. Barnes, Y. Matsuki, P.P. Woskov, B. Corzilius, R.G. Griffin, and R.J. Temkin, *J. Magn. Reson.* 210 (2011) 16–23.
44. E.A. Nanni, S.K. Jawla, M. A. Shapiro, P.P. Woskov, and R.J. Temkin, *J. Infrared and Millimeter Waves.* 33 (2012) 695–714.